DAΦNE TECHNICAL NOTE

INFN - LNF, Accelerator Division

Frascati, August 2, 1996

Note: **MM-19**

THE "SHORT" DIPOLES OF THE DAΦNE MAIN RING ACHROMATS

B. Bolli, N. Ganlin, F. Iungo, F. Losciale, M. Modena, M. Paris,
M. Preger, C. Sanelli, F. Sardone, F. Sgamma, M. Troiani

1. Introduction

The first prototype of the Parallel End Short (PES in the following) Dipole of the Main Rings, built by ANSALDO Energia, arrived at Frascati on August 21, 1995, and the magnetic measurements started on September 4. This first magnet was delivered by ANSALDO without backleg coils and other not essential equipment (shields, temporary cooling hoses, alignment sockets, painting, etc.), as expressly requested by INFN, to test and verify the main magnetic characteristics of the magnet before releasing the required approval for the series production. The magnet was tested hydraulically, thermally, electrically and magnetically.

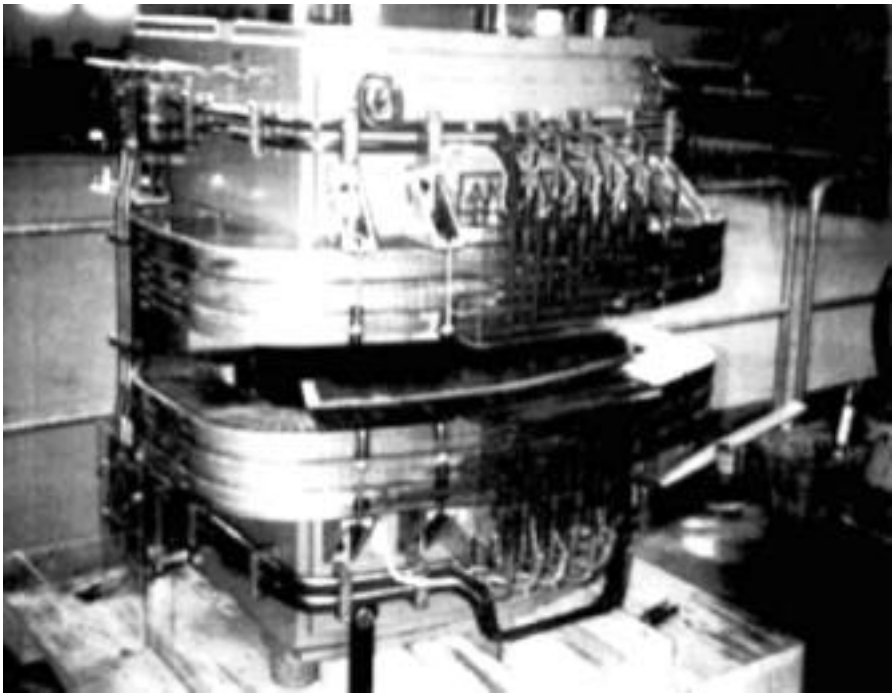

Figure 1.1 - The Parallel End Short (PES) dipole prototype

Some minor bugs were found and fixed; the approval for series production was released on September 22, 1995. The magnetic measurements aimed at the optimization of the pole end caps profile, to reach the required field integral and sextupole minimization were performed and the PES dipole prototype was shipped back to ANSALDO on November 13, 1995. At the same time the discussions on how to realize the Sector Like Short (SLS in the following) dipole prototype went on and on May 22, 1996, the SLS Dipole Prototype was delivered to Frascati as well. After some magnetic measurements, INFN released the authorization for the SLS Dipoles series production on June 6. Figures 1.1 and 1.2 show the PES and SLS Dipole Prototypes respectively. Table I gives their main parameters.

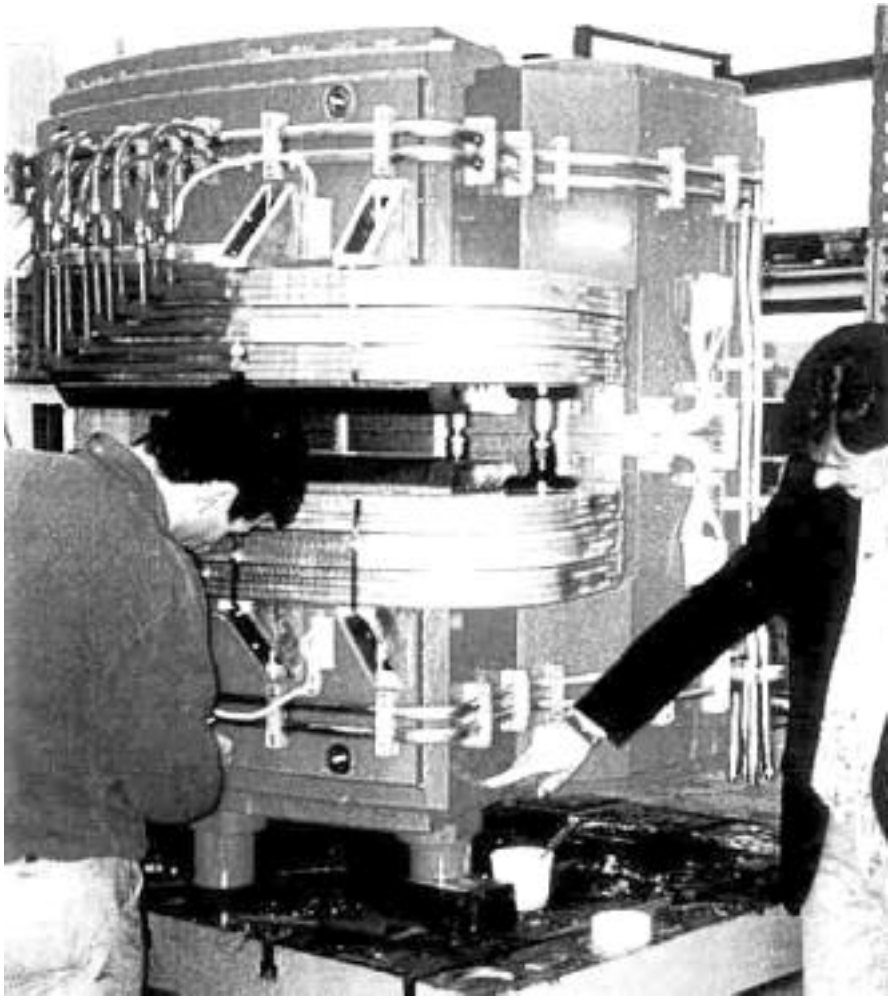

Figure 1.2 - The Sector Like Short (SLS) dipole prototype

Table I - Short dipole prototypes parameters.

	units	PES	SLS
Energy	MeV	510	510
Nominal current (@512 MeV)	A	266.2	266.2
Nominal field (design)	T	1.214	1.214
Measured field	T	1.221	1.207
Deflection Angle	deg	40.5	40.5
Maximum current ≈ 740 MeV	A	621.95	621.95
Max. measured field ≈ 740 MeV	T	1.76	1.78
Field integral on particle trajectory	T.m	1.2068	1.2068
Magnetic Length (Design)	m	0.99	0.99
Measured length ∫(B/Bo)∗dl	m	0.988	1.002
Magnet gap	mm	75.6	75.6
Turns per pole		144	144
Copper Conductor	mm∗mm	12∗12	12∗12
Cooling Hole Diameter	mm	7	7

2. Electrical, mechanical and thermal measurements

The resistance of the main coils and backleg coils of the PES and SLS dipole prototypes were measured by means of a micro-ohm-meter (AOIP mod. OM 20) at room temperature (23°C).

The measured values were:

	Main Coils [mΩ]	Backleg Coil[mΩ]
PES Dipole	145.4	770.0
SLS Dipole	142.4	800.0

The same measurements were accomplished using the Volt-Ampere method and the following data were measured:

PES Dipole	Main Coils	101 V @ 620 A	corresponding to 163 mΩ
	Backleg Coil	7.7 V @ 10 A	corresponding to 770 mΩ
SLS Dipole	Main Coils	38.2 V @ 266.2 A	corresponding to 144 mΩ
	Backleg Coil	8.3 V @ 10 A	corresponding to 832 mΩ

The resistance of the Main Coils of the PES Dipole was measured at 620 A with a temperature increase of the cooling water of about 30 °C. Scaling this value we get a resistance of 146.1 mΩ, in good agreement with the value measured at room temperature.

The inductance and resistance of the magnets were also measured by means of a LCR meter (LCR meter HP 4284 A) at different frequencies. The results are shown in figure 2.1 and 2.2. The corresponding dc values may be extrapolated from these data. They are consistent with the measured ones, given above.

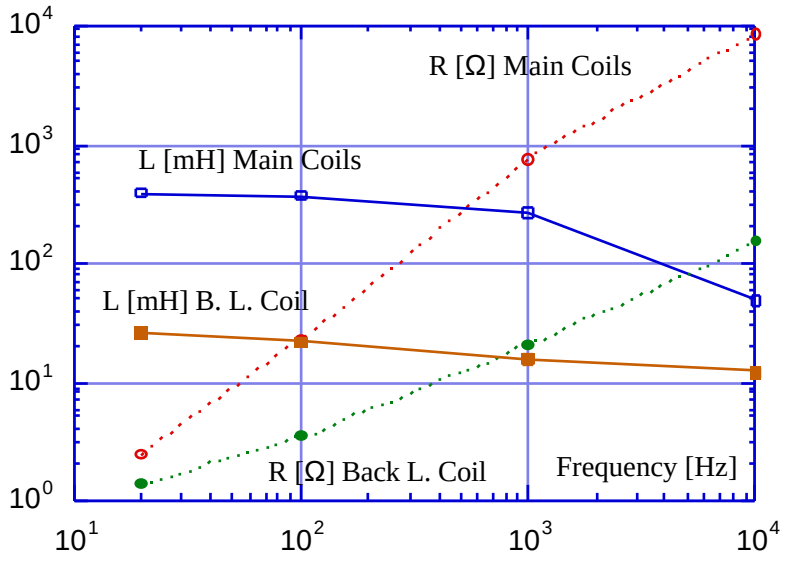

Figure 2.1 - Resistance and Inductance versus frequency of the Main Coils and Backleg Coil (B.L.) of the PES Dipole Prototype.

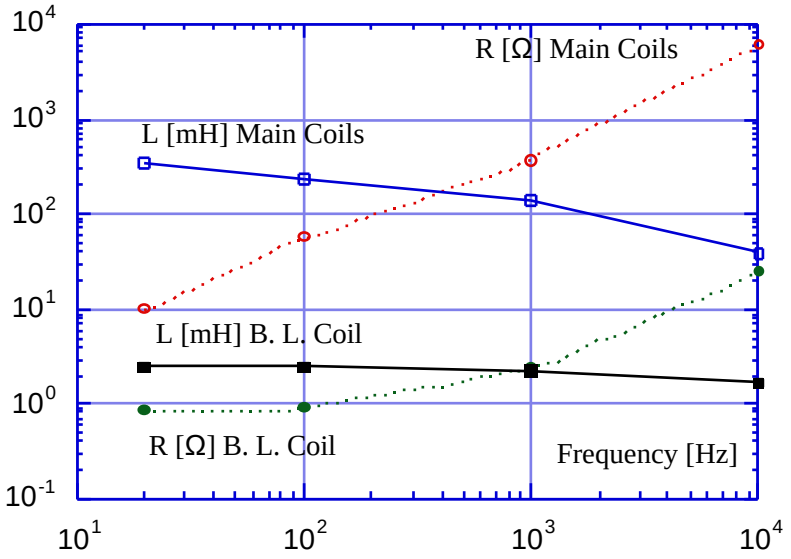

Figure 2.2 - Resistance and Inductance versus frequency of the Main Coils and Backleg Coil (B.L.) of the SLS Dipole Prototype.

The magnet were also thermally characterized and figures 2.3 and 2.4 show the worse thermal figure for the PES and SLS Dipole respectively.

The coupling between the Main Coils and the Backleg Coil was also measured. Figure 2.5 shows the voltage induced on the Back Leg Coil when the current flowing into the Main Coils (620 A) is suddenly switched off. The maximum induced voltage is about 20 V (the vertical scale of 50 V/div. must be divided by 10, the amplification factor of the probe).

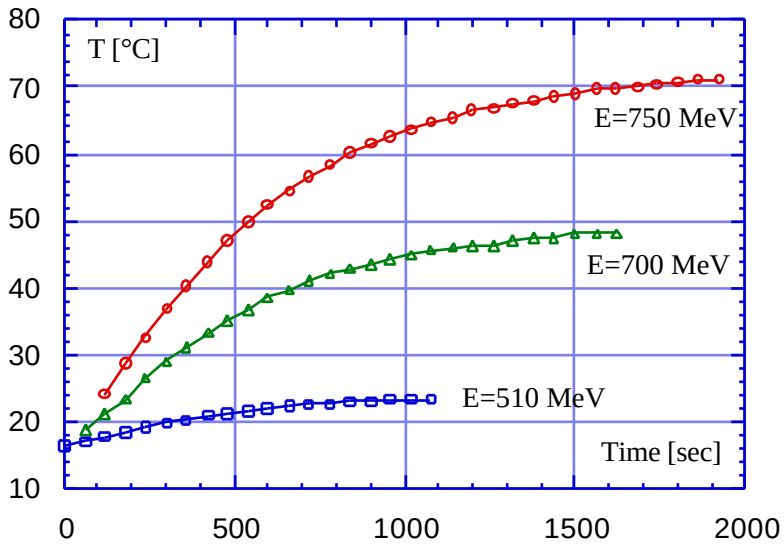

Figure 2.3 - Outlet water temperature increase versus time at different energies for the PES Dipole Prototype.

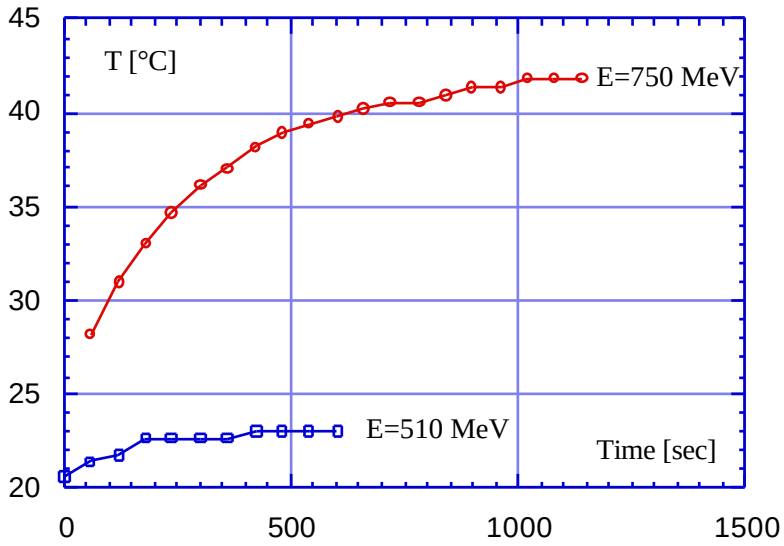

Figure 2.4 - Outlet water temperature increase versus time at different energies for the SLS Dipole Prototype.

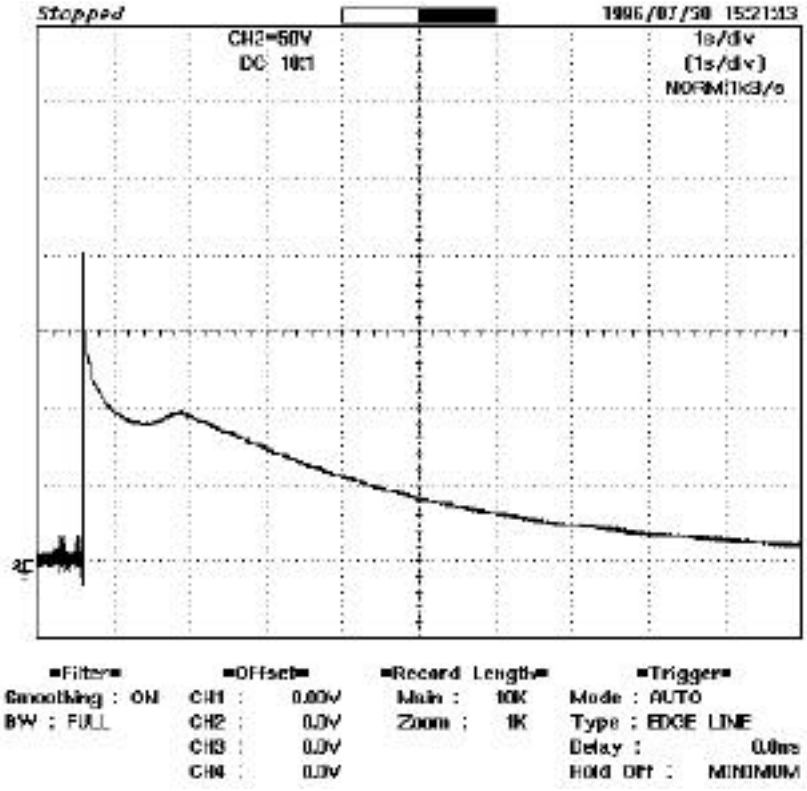

Figure 2.5 - Voltage induced on the Backleg Coil.

We have also measured the gap reduction due to the magnetic pressure versus the excitation current. Figure 2.6 shows the gap reduction found by measuring the movement of the upper pole with respect the lower one. At the nominal energy of 510 MeV a gap reduction of about 100 µm is expected. As shown on the figure, the variation is more or less linear with the current and at the maximum current of 620 A the gap reduction is about 200 µm.

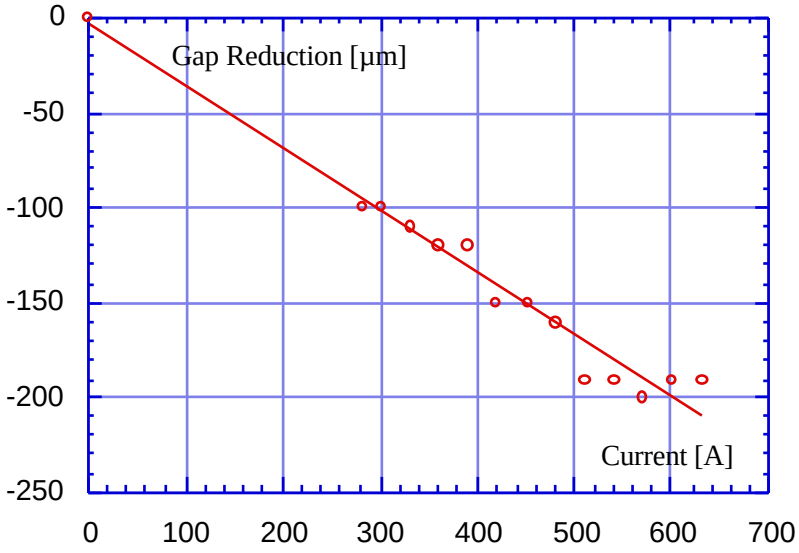

Figure 2.6 - PES Dipole, gap reduction versus excitation current.

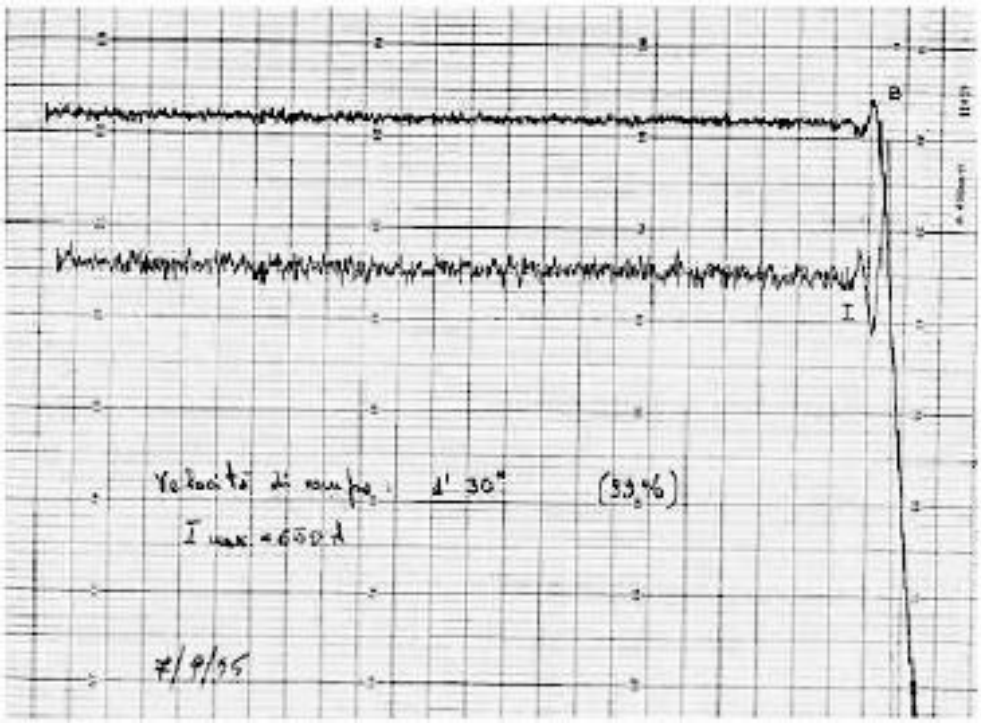

Figure 2.7 - Excitation current (lower trace) and magnetic field (upper trace) versus time before the stress test. Test current = 650A; ramp speed from 0 to 650A = 90 seconds.

Since the pole surfaces of the dipoles have been machined to get the required planarity and parallelism, the PES dipole prototype has been tested to verify that short circuits among the laminations caused by the pole surface machining do not lead to degradation, increasing their effect and inducing micro-discharges among the laminations due to the eddy currents during magnet ramping.

The magnet was therefore tested by ramping up and down from zero to the maximum current (I_{max} =650 A) and from I_{max} to zero continuously for three days, at the maximum ramp speed allowed by the power supply (90 sec). The magnet was tested with a number of standardization cycles equivalent to about 5 years of normal operation.

Figure 2.7 shows the excitation current and the magnetic field at the top of the ramp at the beginning of the test, while figure 2.8 shows the same quantities at the end of the test. The two curves look almost identical and there is no evidence of any degradation phenomena. Following the result of this test, the machining procedure was approved and approval for series production released.

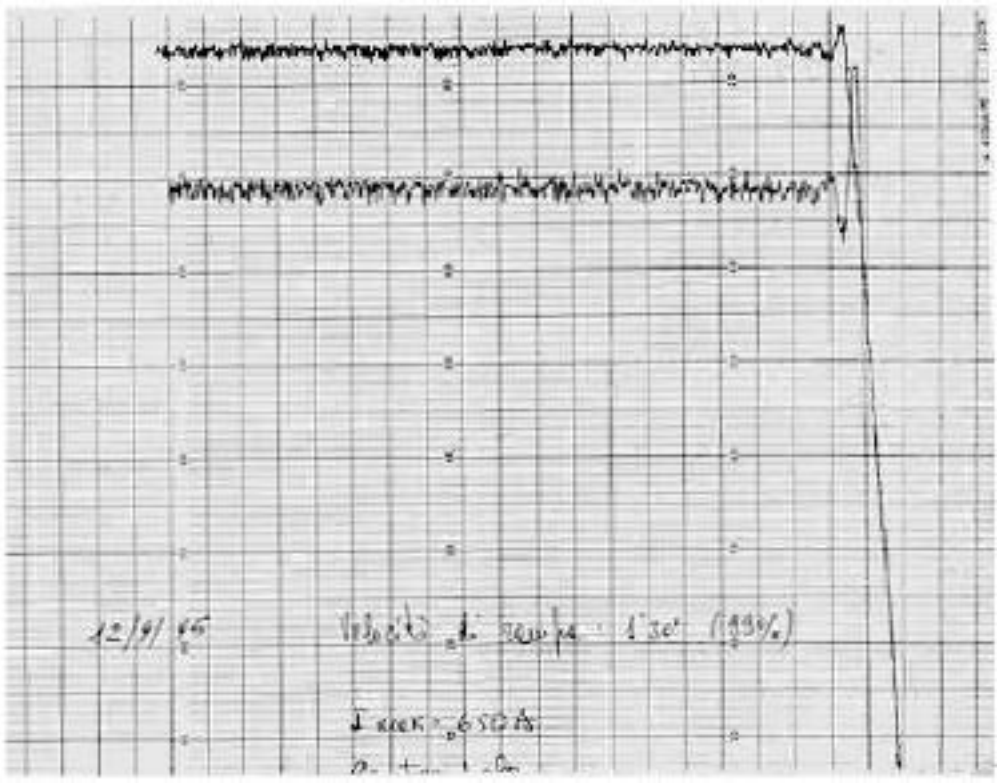

Figure 2.8 - Excitation current (lower trace) and magnetic field (upper trace) versus time after the stress test. Test current = 650A; ramp speed from 0 to 650A = 90 seconds.

3. Magnetic measurements

We report here the results of the magnetic measurements performed on the prototype of the PES dipole in May and those on the SLS prototype in June and July 1996. The optimization of the end cap shape on the PES magnet, however, has been performed on the PES prototype from September to November 1995. As said before, the PES dipole was delivered on August 1995 for a first set of measurements. After these measurements the magnet was shipped back to Ansaldo to be completed. Ansaldo had to dismount the main coils to wind the backleg correction coils and to paint the magnet. When the magnet was delivered the second time, we made a complete new set of magnetic measurement to be sure that dismounting and mounting the main coils did not change the magnetic field distribution.

3.1 - Optimization of the steel length

The magnetic length and the shim shape have been optimized following the procedure adopted for the DAΦNE Accumulator dipoles [1]. In the present case, being the Main Ring magnets of the "C" type, the measurements were easier, since it was not necessary to rotate the dipoles in order to perform the complete scan of the field. The magnets were positioned with their symmetry axis perpendicular to the 2.5m long "longitudinal" movement of the Hall probe positioning system. The 1m "transverse" movement parallel to the magnet symmetry axis covers easily the required good field region. However, due to the absence of field clamps, the magnets exhibit rather long field tails outside the end caps, especially at the maximum excitation current, so that in some cases it was not possible to extend the measurement at a distance where the field could be defined as negligible.

During the magnetic length optimization procedure performed on the removable end caps it appeared that the field at the magnet center changes slightly as a function of the overall steel length. Figure 3.1 shows therefore the result of the excitation curve measured on the PES dipole in its final configuration. The nominal operating point for the magnet, corresponding to 0.51 GeV beam energy is just at the separation point between the linear and the saturation regions.

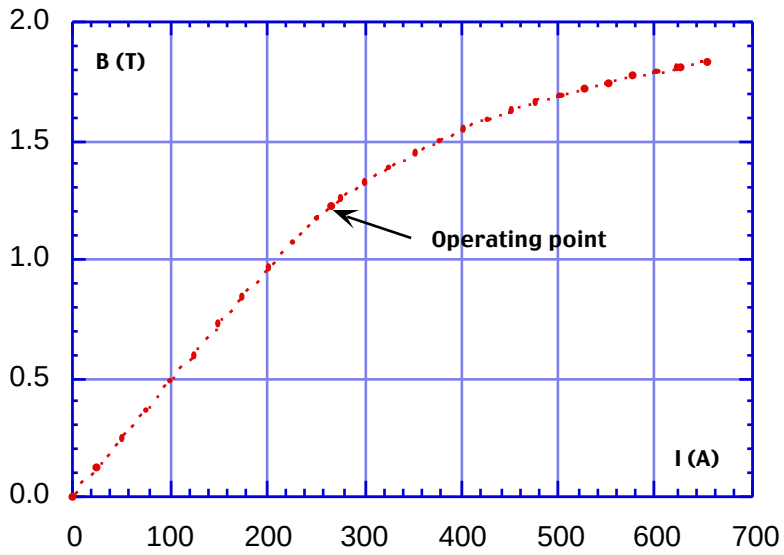

Figure 3.1 - Vertical component of the field at the magnet center versus coil current.

The optimization of the steel length has been performed by cutting the iron of the removable end caps in successive steps and measuring the field map at each cut. Let us remind that in the case of short magnets, where the fringing field region is in the same order of the steel length, it is not correct to simply define the magnetic length as the field integral along the nominal beam trajectory divided by the field value at the magnet center. Actually, the particles are deflected towards the inside of the machine by the fringing field well before the nominal dipole edge, and follow therefore a trajectory displaced from the nominal one by a non negligible amount. The choice of the steel length comes in this case from a compromise between the opportunity of exploiting in the best way the good field region, keeping the above mentioned displacement as small as possible, and the need to keep the excitation current below the value where the steel saturation becomes strong.

We have therefore measured the field along the nominal trajectory, namely a circular sector with the nominal bending radius (1.40056 m) and angle (40.5°) plus two straight lines tangent to the sector at its end points. The same longitudinal scan has been performed along 8 other trajectories, parallel to the first one, in such a way that for each measured point on the nominal trajectory there are other 8 measured points along a line perpendicular to the nominal trajectory at the same longitudinal position. The points were measured in steps of 10 mm along the longitudinal direction on the nominal trajectory and in steps of 10 mm as well in the transverse one, so that the mesh of measured field values extends by ±40 mm in the transverse direction. By interpolating the measurements in this mesh, it is possible to integrate the equations of motion of the particles and find the real trajectory followed by the beam, which depends on the steel length of the magnet. It is assumed that the particles start from the nominal trajectory, a straight line tangent to the nominal bending arc; the energy of the particles is varied until the bending angle is exactly the nominal bending one; of course in this case the output trajectory is a straight line at the nominal bending angle from the input one, but there may be an offset from the ideal output line, due to any possible asymmetry of the field with respect to the symmetry axis of the magnet.

Starting from the original removable end cap, the dipole steel length has been shortened in successive steps by 5, 10, 15 and finally by 20 mm on each side. Figure 3.2 shows the distance between the real and nominal trajectories calculated from the corresponding field maps. All measurements were performed at the same excitation current (266.24 A) in the magnet coil. It can be observed from this figure that this distance decreases when the total steel length is shortened. In addition, the output trajectory is displaced by ≈0.3 mm from the nominal one. It is worth reminding that the PES prototype was delivered to LNF the first time without alignment sockets, and that the magnet was therefore positioned with respect to the Hall probe by detecting by optical means the position of the yoke boundaries. When the complete magnet was delivered in May 1996, this offset was significantly reduced.

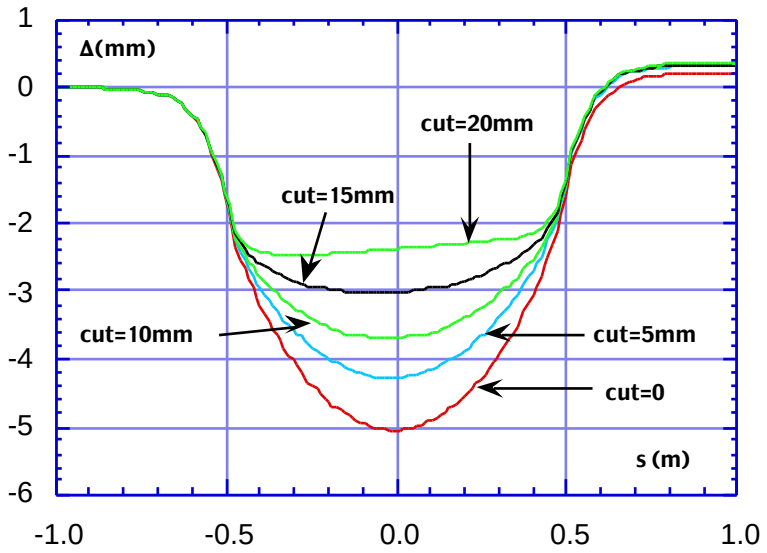

Figure 3.2 - Distance between real and nominal trajectories in the PES dipole for different depths of the cut performed on the removable end caps.

Figure 3.3 shows, as a function of the cut depth, the particle energy corresponding to the nominal 40.5° deflection, while Fig. 3.4 gives the ratio of the measured field at the magnet center to the nominal field at that energy. The choice of the final cut at 20 mm on both sides of the magnet, for the PES dipole, has been made as a compromise between an acceptable displacement of ≈2.5 mm of the beam from the magnet center and a reduction of ≈2% of the energy for the same excitation current. In addition, as shown in Fig. 3.4, the field at the magnet center in the final configuration is almost equal to the nominal one.

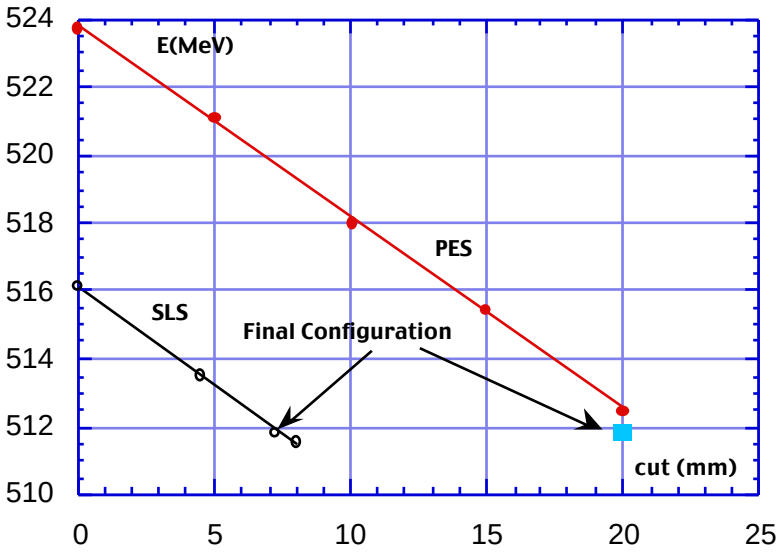

Figure 3.3 - Particle energy corresponding to the nominal deflection versus cut depth.
The square corresponds to the value found on the PES prototype during the second set of measurements.

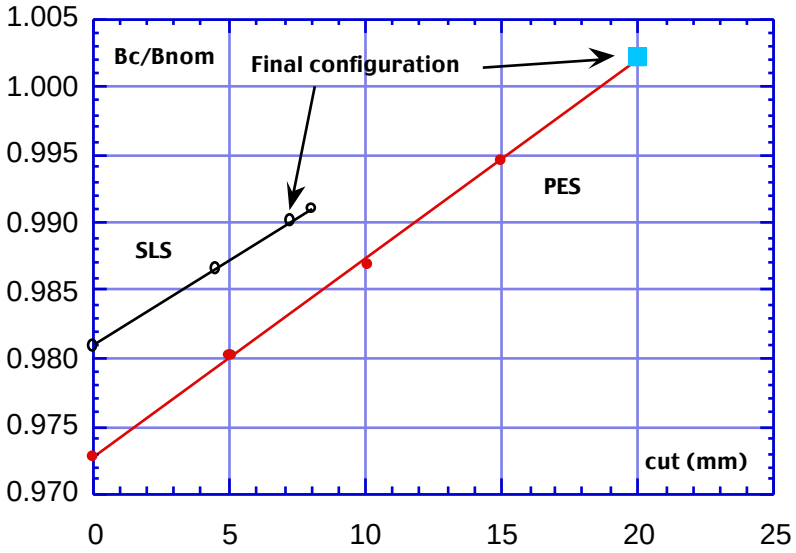

Figure 3.4 - Measured field at the magnet center divided by the nominal field corresponding to the particle energy versus cut depth.
The square corresponds to the value found on the PES prototype during the second set of measurements.

An unwanted consequence of the displacement between the real and nominal trajectories in the dipole is the overall shortening of the particle orbit, which affects the nominal revolution frequency of the ring. This effect is in any case rather small with respect to the tuning range of the RF cavities. However, it may affect the conditions under which it is possible to obtain the required synchronization between the Main Rings and the Accumulator [1]. Preliminary results from the Accumulator commissioning indicate that the machine acceptance is sufficient to compensate for this small mismatch.

Figure 3.5 shows the shortening of the trajectory as a function of the cut depth. Also in this case the harmful effect is reduced when the cut depth increases.

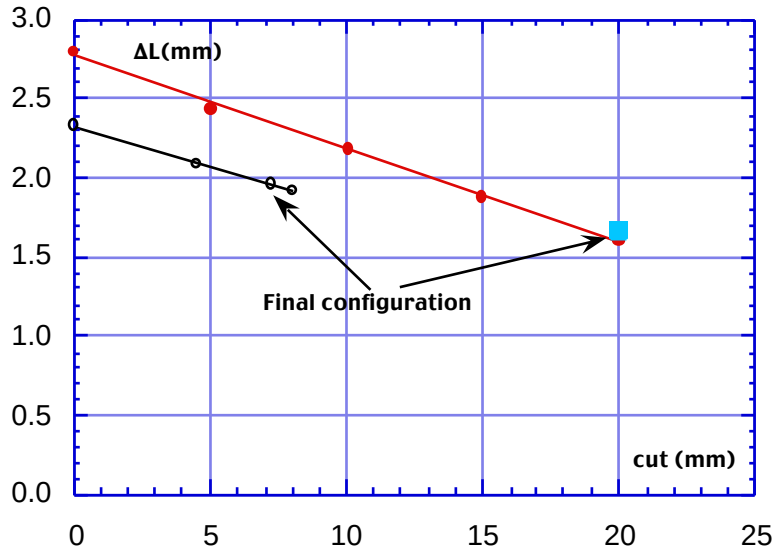

Figure 3.5 - Shortening of the beam trajectory length with respect to the nominal one versus cut depth. The square corresponds to the value found on the PES prototype during the second set of measurements.

Once chosen the steel length for the first dipole, there is no more choice for the others, because all the dipoles of a single DAΦNE Main Ring are powered in series. The field integrals of the PES and SLS dipoles must therefore be the same at all operating energies. This is made possible by means of independent backleg correction windings on each magnet (described in the following). However, we have set the reasonable constraint of making the field integrals the same with negligible current in the correction windings at the nominal operating energy of the collider.

We required therefore that, at the same excitation current set for the PES dipole, the beam energy on the real trajectory calculated from the field maps for the nominal deflection be the same for both the PES and SLS magnets. The behaviour of the beam energy for the SLS dipole as a function of the cut depth is given in Fig. 3.3. The square point in the figure corresponds to the measurement performed on the PES prototype during the second set of measurements: the small difference between the two energy values at the same cut comes from the better alignment procedure performed the second time on the prototype, delivered to LNF with the final alignment sockets. The second value for the PES dipole was used to make the energies of the PES and SLS dipoles equal. It can be observed from Fig. 3.3 that a cut of 8 mm was performed on the SLS dipole, which made the energy lower than the desired value; this was due to a mistake in the extrapolation, which was corrected by adding a 0.75 mm thick iron lamination between the yoke and the end cap, as shown in Fig. 3.6.

From Fig. 3.4 it can be noticed that the field at the magnet center is ≈1% lower than the nominal one for the SLS dipole, and, from Fig. 3.5, that the orbit shortening is larger than in the PES dipole as well.

Figure 3.7 shows the difference between the real and nominal trajectories for the both the PES and SLS magnets in their final configuration: also in this case the displacement for SLS is larger than in PES.

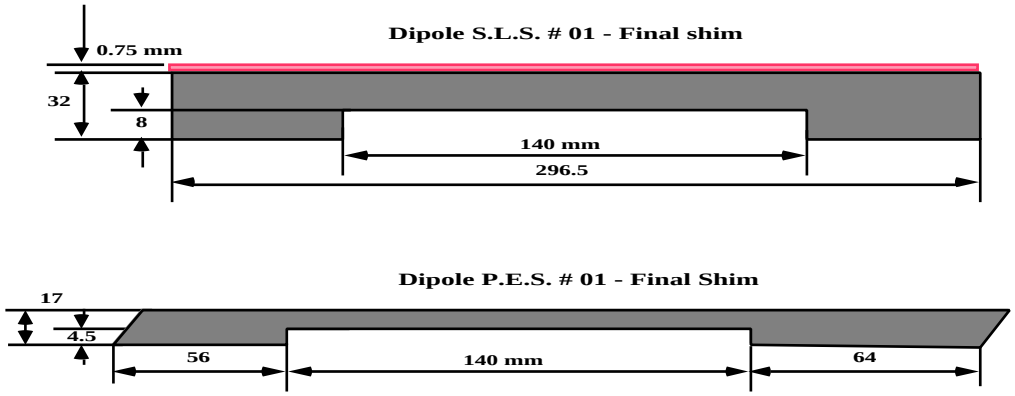

Figure 3.6 - Final end cap configuration for PES and SLS dipoles (not in scale)

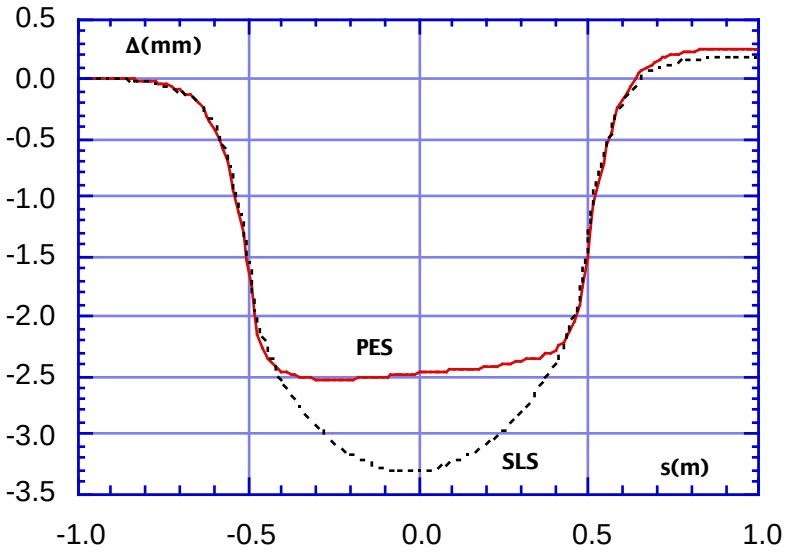

Figure 3.7 - Displacement between real and nominal trajectories in the dipoles in their final configuration (full line = PES dipole, dotted line = SLS dipole)

3.2 - Optimization of the sextupole contribution.

It has been shown in [1] that the fringing field region of short magnets can be seriously affected by sextupole-like contributions. We have therefore studied the behaviour of the second order term of the polynomial fit to the 9 field values measured at each azimuthal position in the magnets as a function of the shim realized on the removable end caps. The shim is characterized by the width and depth of the rectangular cut on the end cap, as shown in Fig. 3.6, where both shims have a width of 140 mm. The optimum depth is 8 mm for the SLS dipole, 4.5 mm for the PES one.

Figure 3.8 plots the second order term of the transverse expansion for the two dipoles with the original end caps without shims. It appears that for the PES dipole there are two peaks of opposite sign in each fringe, while for the SLS magnet the peaks are negative, as in the case of the Accumulator dipoles [1], but much smaller than both in the PES and Accumulator

There is no significant sextupole contribution inside the magnets, due to the large width of the poles. In the case of the SLS the integral of the second order term along the nominal trajectory was -0.97 T/m, while for the PES this value was quite similar (-0.87 T/m), in spite of the larger peaks, due to the cancellation of the opposite sign peaks.

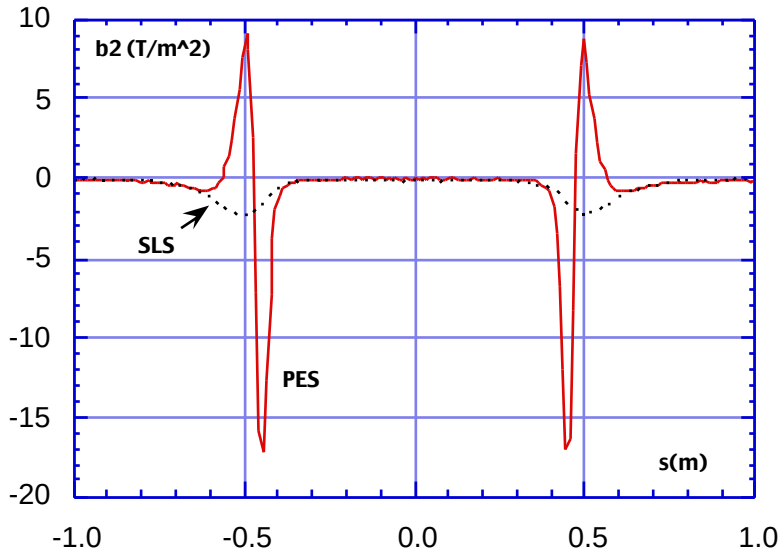

Figure 3.8 - Second order term of transverse expansion versus longitudinal position without shims (full line = PES dipole, dotted line = SLS dipole).

Although these sextupole contributions were small with respect to the overall contributions to the chromaticity of the Main Rings, we have tried to reduce them as far as possible by applying the shimming technique already adopted for the Accumulator dipoles [1]. In the case of the PES dipole three different shim depths were tried (5 mm, 4 mm and finally 4.5 mm, see Fig. 3.6). In the SLS case the final configuration was found after two trials (4.5 mm and 8 mm). Figure 3.9 shows the dependence of the integrated second order term of the transverse expansion on the shim depth. Figure 3.10 gives the same coefficient versus the longitudinal position in the final configuration, where both magnets exhibit now peaks of alternating polarity, with a good cancellation of the opposite effects.

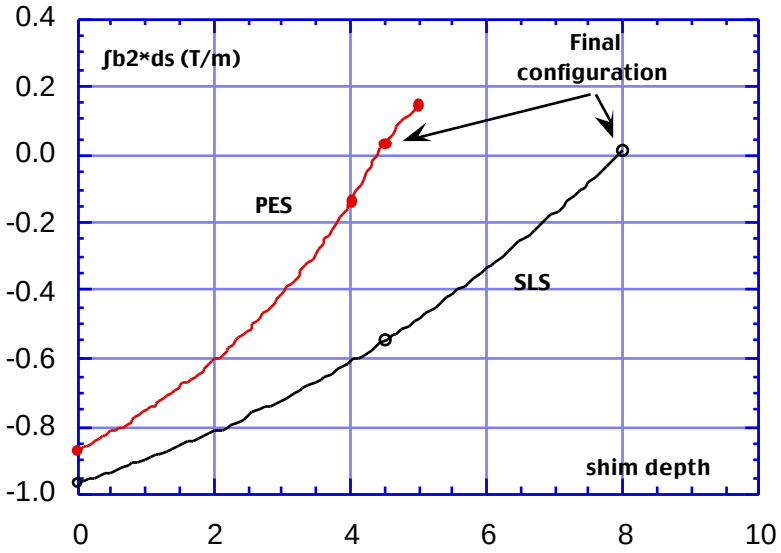

Figure 3.9 - Integrated second order term of transverse expansion versus shim depth.

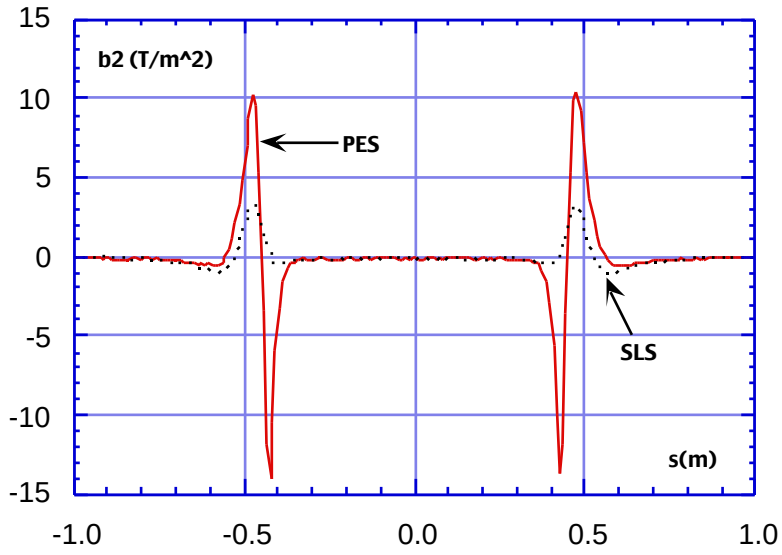

Figure 3.10 - Longitudinal dependence of the second order term of the transverse expansion in the final configuration of the two dipoles (full line = PES dipole, dotted line = SLS dipole)

3.3 - Other terms of the transverse expansion in the final configuration.

Figure 3.11 shows the zero order term of the transverse expansion, namely the field value on the nominal trajectory at the nominal working point for the two dipole prototypes. At constant field integral (as explained before), a slight difference between the two fields can be observed: the sector like magnet, as expected, has a flatter field under the poles and a slightly steeper fringe.

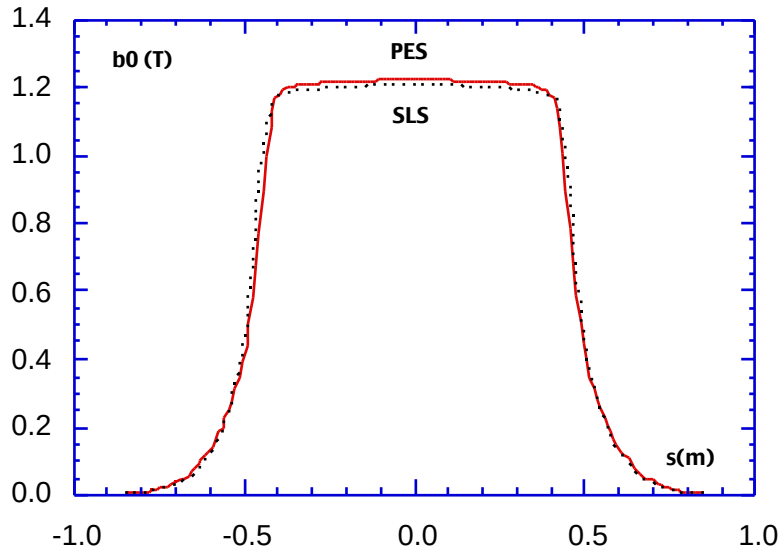

Figure 3.11 - Zero order term of transverse expansion (full line = PES dipole, dotted line = SLS dipole)

The first order term, the point-to-point value of the gradient, is shown in Fig. 3.12. The parallel end magnet has two large negative peaks in the fringing region. Its integrated value of -0.77 T is smaller than its theoretical value for an ideal magnet with parallel ends (-0.86). The difference is due to a small effect coming from the fact that the magnet yoke is shorter than the nominal magnetic length, while the angle between the opposite end caps is the nominal one. This introduces a small quadrupole-like contribution of the opposite sign: this happens, as it can be observed from Fig. 3.12, also for the sector like magnet, where the integrated quadrupole contribution is 0.026 T.

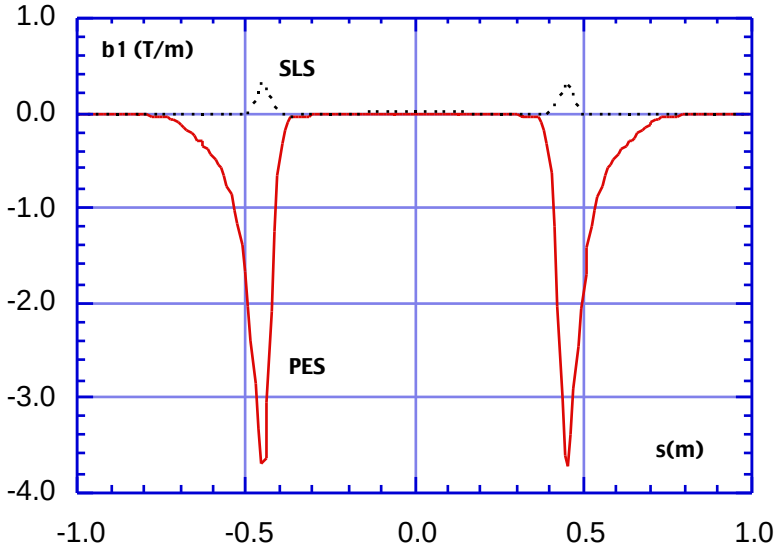

Figure 3.12 - First order term of transverse expansion (full line = PES dipole, dotted line = SLS dipole)

Figures 3.13 and 3.14 show, respectively, the third and fourth order terms of the transverse expansion. As expected, there is a non negligible octupole term in the PES dipole fringing field, coming from the distortion of the linear term. However, the integrated octupole term (≈6 T/m^2) is still quite small, and should not create harmful effects on the beam dynamics. The fourth order term is almost the same for the two dipoles, one order of magnitude smaller than in the case of the Accumulator one [1].

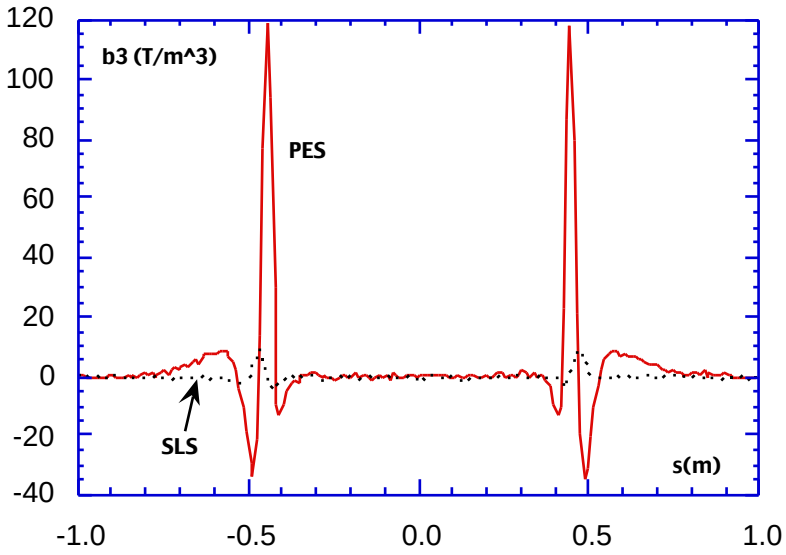

Figure 3.13 - Third order term of transverse expansion (full line = PES dipole, dotted line = SLS dipole)

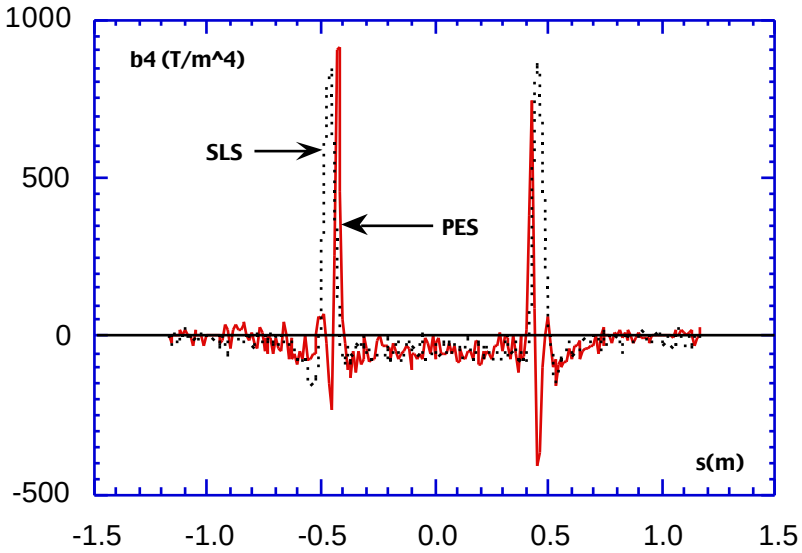

Figure 3.14 - Fourth order term of transverse expansion (full line = PES dipole, dotted line = SLS dipole)

3.4 - Dependence on the excitation current.

Both magnets, as explained in this Section, have been optimized at the nominal operation energy of DAΦNE (0.51 GeV per beam), with the steel length determined by the condition of making the field integrals on the real trajectory the same. However, the main characteristics of the field have been investigated also for different operating conditions, at other 5 fixed currents. Table V shows the beam energy calculated from the integration of the field values on the real trajectories derived from the corresponding field maps.

Table V - Beam energy versus excitation current

Current (A)	E_{PES} (MeV)	E_{SLS} (MeV)	$\Delta E_{PES-SLS}$	$\Delta E_{backleg}$
225.40	449.98	452.35	-2.37	±4.34
266.24	511.82	511.87	-0.05	±2.56
300.96	551.04	552.54	-1.50	±1.97
354.70	601.33	604.08	-2.75	±1.55
502.90	694.77	693.75	1.02	±0.76
621.95	738.97	737.04	1.93	±0.59

The maximum difference between the two dipoles has been found at a field corresponding to ≈0.6 GeV. Each dipole is equipped with a backleg coil powered by a bipolar supply capable of delivering ±10A. The field value at the magnet center has been measured on each prototype at all the above mentioned excitation currents as a function of the current in the winding. The energy change introduced by the correction winding depends on the current in the main coil, due to the saturation shown in Fig. 3.1, and is listed in the last column of the Table: it can be noticed that the energy difference between the two magnets can be always compensated, but for the extreme point near 0.74 GeV. It should be kept in mind that at energies higher than 0.6 GeV the compensation requires the use of both the SLS and PES coils with opposite signs. The compatibility with the "long" dipoles, still to be delivered by ANSALDO to LNF, must therefore be carefully checked.

Figure 3.15 shows the ratio between the field measured at the magnet center and the nominal field at the corresponding energy. For sake of simplicity, we plot all the following results of magnetic measurements versus the beam energy corresponding to each excitation current.

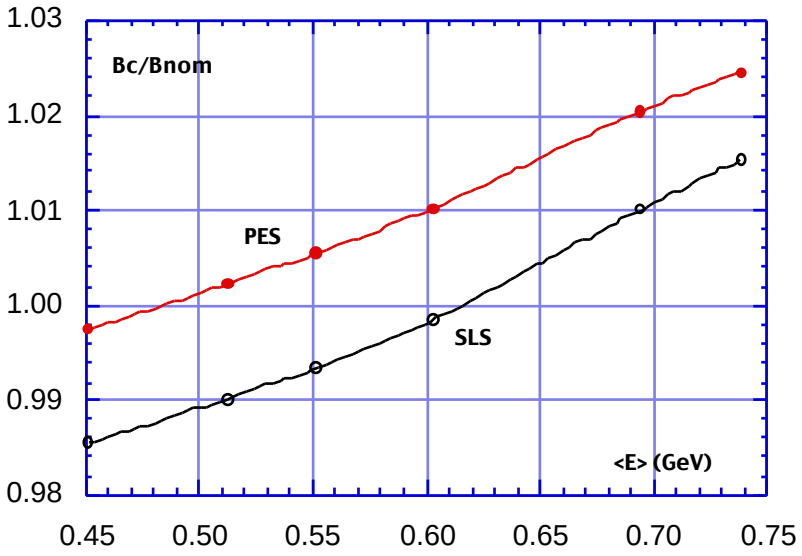

Figure 3.15 - Field at magnet center divided by nominal field versus energy.

The integrated first order term of the transverse expansion is given in Fig. 3.16. The absolute value of the integrated gradient increases linearly with beam energy, as expected, for the PES dipole. The small spurious effect for the SLS, described in the preceding subsection, is almost constant. The reason can be searched in the compensation of the geometric effect with the saturation of the field in the end caps.

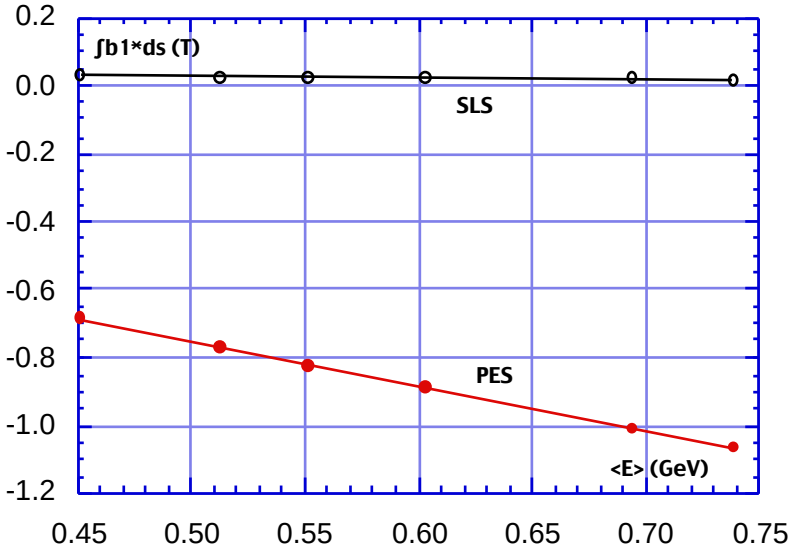

Figure 3.16 - Integrated first order term of the transverse expansion versus energy.

Figures 3.17, 3.18 and 3.19 show the corresponding behaviours for the second, third and fourth order terms of the transverse expansion.

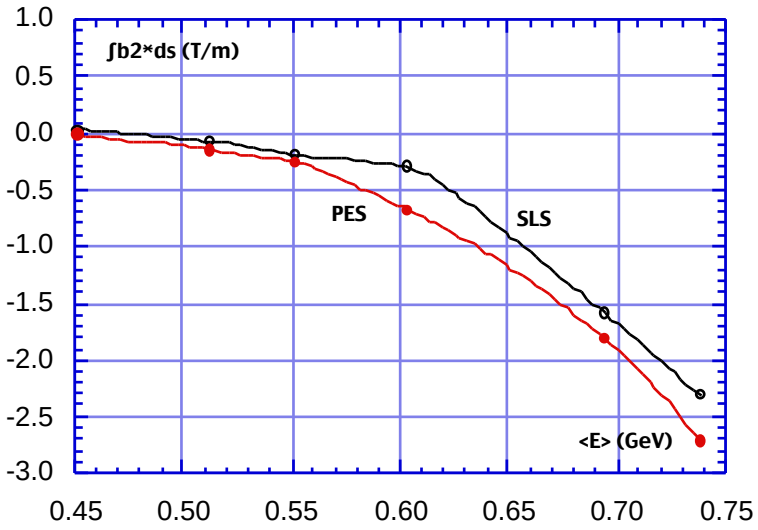

Figure 3.17 - Integrated second order term of the transverse expansion versus energy.

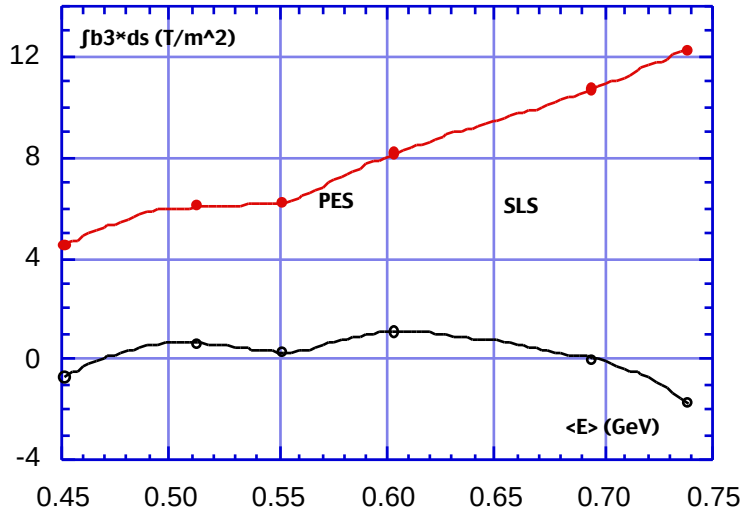

Figure 3.18 - Integrated third order term of the transverse expansion versus energy.

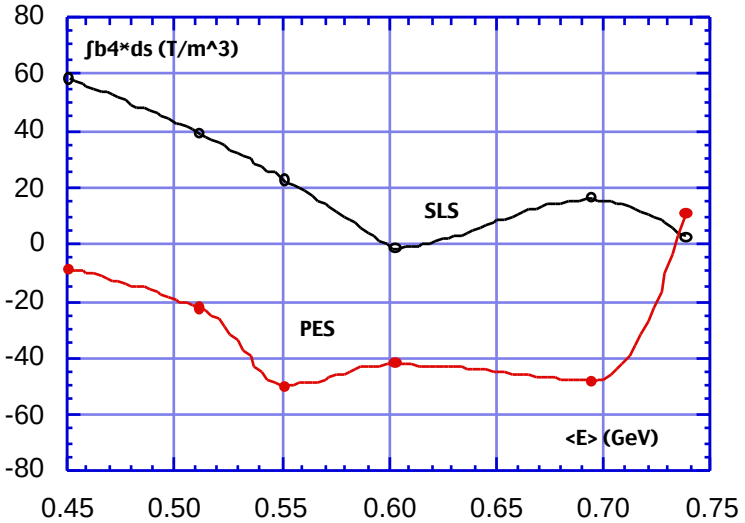

Figure 3.19 - Integrated fourth order term of the transverse expansion versus energy.

The last three figures give the dependence on beam energy of the main parameters of the real trajectory followed by the particles in the magnets.

Figure 3.20 plots the maximum distance between the real and nominal trajectory in the magnet.

Figure 3.21 gives the shortening of the path followed by the particles with respect to the nominal orbit length in the dipole. Both these harmful effects decrease with increasing energy.

Figure 3.22 shows the offset of the trajectory at the exit from the magnet.

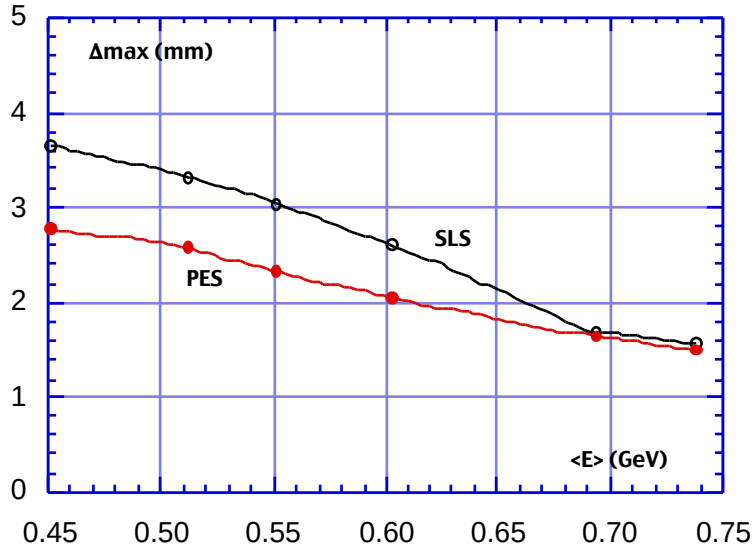

Figure 3.20 - Maximum displacement between real and nominal trajectories versus energy.

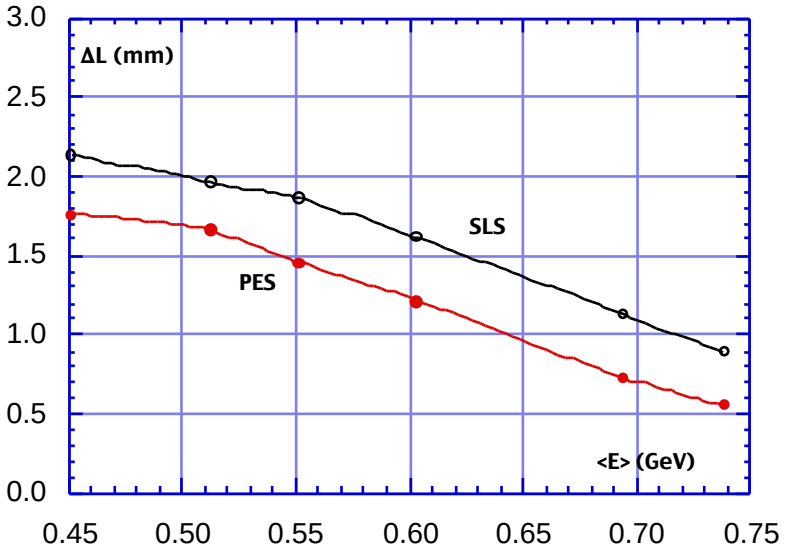

Figure 3.21 - Orbit shortening per magnet versus beam energy.

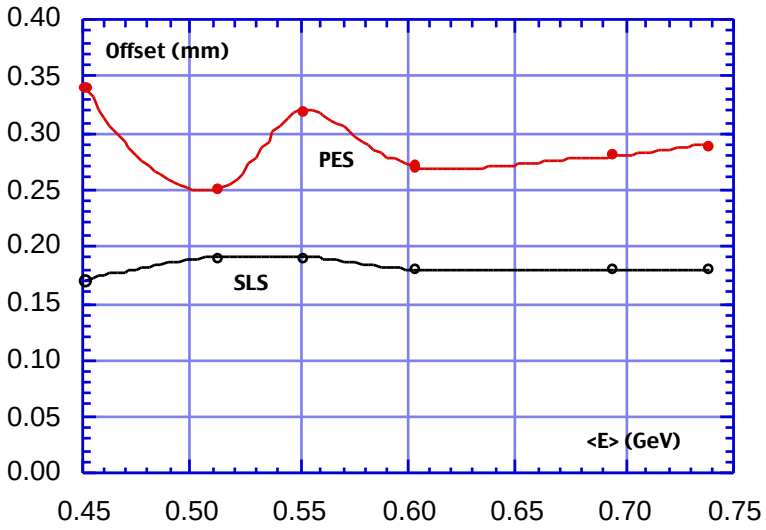

Figure 3.22 - Offset of particle trajectory at the output from the magnet.

3.5 - Stray fields

As mentioned before, at large excitation current, the available span of the Hall probe positioning system was not sufficient to measure the stray field of the magnets completely. Fig 3.23 shows the field on the nominal trajectory outside the magnet, namely a straight line at 20.25° with respect to the symmetry axis of the PES dipole. It can be seen from the figure that when the current is larger than 300 A (well above the nominal operating point at 266 A), there is a non negligible negative "overshoot" in the stray field. The field integrals given above do not take into account the missing part of the field; however, at the distance where it was impossible to measure the field, ≈70 cm from the nominal magnet edge, the field of the magnets in the real machine interferes with those of the neighbouring quadrupoles, so that it is difficult to estimate reliably the effect of the stray fields. Fig. 3.24 shows the same quantities for the SLS dipole. The stray field is smaller than in the PES case.

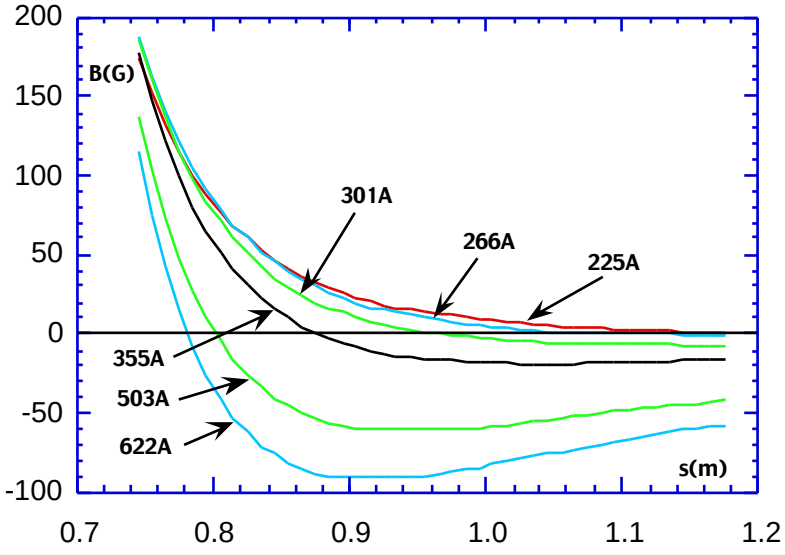

Figure 3.23 - Stray field outside the PES dipole for different excitation currents. The horizontal axis is the distance from the magnet center.

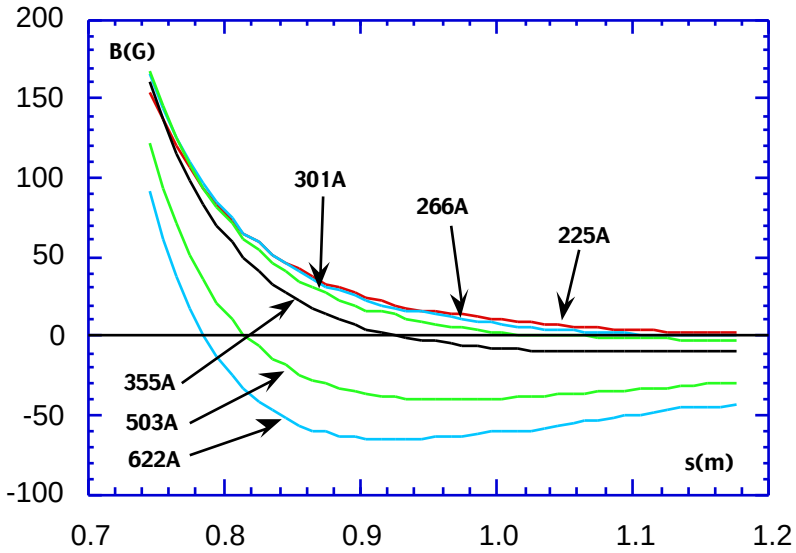

Figure 3.24 - Stray field outside the SLS dipole for different excitation currents. The horizontal axis is the distance from the magnet center.

A wide rough map of the field has been performed for the PES dipole in the region outside the Hall probe positioning system range, in order to check, in particular on the gap side, the amount of stray field in the vicinity of the second ring of the collider. Near the maximum excitation current (@ 620A) the maximum field in the direction perpendicular to the nominal trajectory at the magnet center (corresponding to the negative maximum of the overshoot) is ≈90 G at a distance of 70 cm, while it drops to ≈50 G at 1 m, the typical distance of the dipole yoke of the second ring from the gap center of the first one. The effect is much smaller at 330A, near the operating point of the collider, where both the above mentioned values are below 10 G.

References

[1] A. Battisti, B. Bolli, F. Iungo, F. Losciale, M. Paris, M. Preger, C. Sanelli, F. Sardone, F. Sgamma, M. Troiani, S. Vescovi - "Measurements and tuning of DAΦNE Accumulator dipoles" - DAΦNE Technical Note MM-9 (29/8/1995).